Formation of endogenous MgO and MgAl2O4 particles and their possibility of acting as substrate for heterogeneous nucleation of aluminum grains

Kim, Keehyun

DOI:
10.1002/sia.5726

Document Version
Publisher's PDF, also known as Version of record

Citation for published version (Harvard):
Kim, K 2015, 'Formation of endogenous MgO and $MgAl_2O_4$ particles and their possibility of acting as substrate for heterogeneous nucleation of aluminum grains', *Surface Interface Anal*, vol. 47, no. 4, pp. 429-438. https://doi.org/10.1002/sia.5726

Research article

SURFACE and INTERFACE ANALYSIS

Received: 11 June 2014 Revised: 13 November 2014 Accepted: 14 November 2014 Published online in Wiley Online Library: 22 January 2015

(wileyonlinelibrary.com) DOI 10.1002/sia.5726

Formation of endogenous MgO and $MgAl_2O_4$ particles and their possibility of acting as substrate for heterogeneous nucleation of aluminum grains

KeeHyun Kim*

Aluminum containing 4 wt.% magnesium was oxidized at a temperature for different oxidation times and analyzed by high-resolution electron microscopy. A thin oxidized layer of about 5 μm, which is composed of MgO, forms at short oxidation time and gradually increases. High-resolution microstructures reveal that the oxidized layers are porous regardless of oxidation time. After extended oxidation time, discrete $MgAl_2O_4$ particles formed as a result of the reaction of initially formed MgO, liquid aluminum, and oxygen introduced from air through the porous MgO. Furthermore, it is clear by high-resolution lattice images that $MgAl_2O_4$ particles are covered with thin Al_2O_3, whereas MgO is bonded intimately to aluminum. Therefore, $MgAl_2O_4$ particles that form naturally during oxidation are difficult to act as a direct substrate for nucleation of aluminum grains because of the coverage of Al_2O_3. In contrast, MgO shows the possibility of acting as a substrate for the aluminum nucleation. The formation mechanism of MgO and $MgAl_2O_4$ and their possibility of acting as substrates for nucleation of aluminum grains suggest that atomic level bonding and mismatches of nucleant/nucleus metal should be considered for correct evaluation of the possibility of heterogeneous nucleation of metallic matrix on a potent nucleant. © 2015 The Authors. *Surface and Interface Analysis* Published by John Wiley & Sons Ltd.

Keywords: heterogeneous nucleation; endogenous particle; analytical electron microscopy; focused ion beam; oxidation

Introduction

Wetting between reinforcements and metallic matrix is the most important requirement to obtain uniform dispersion of reinforcements. The wetting can be improved by increasing the surface tension of reinforcements or decreasing that of the matrix and the interfacial energy of reinforcements/matrix.[1,2] The addition of magnesium to molten pure aluminum has proved to enhance the wettability of the ceramic reinforcements[3–5] and changes the oxide film from Al_2O_3 to $MgAl_2O_4$.[6] The interfacial bond of reinforcements/matrix can be improved by the formation of spinels, such as $MgAl_2O_4$ that can promote the bond strength between metals and ceramics.[3,4,6–14] In addition, magnesium reduces the casting fluidity and the surface tension of aluminum melt and acts as a powerful surfactant in aluminum alloys.[1]

Aluminum–magnesium melt can oxidize rapidly because of the formation of magnesium oxide, whereas pure aluminum or aluminum alloys free of magnesium oxidize more slowly at temperatures proper for melt processing.[15–17] This rapid oxidation has been widely studied to prevent or minimize the severe melt loss, unexpected alloy compositional changes from the formation of preferential oxidation of magnesium.[15] In casting, the oxide is easily fractured and entrained into the melt by the turbulence of melt stirring and pouring. Consequently, the oxide causes the formation of hot tearing and porosity and reduces the mechanical properties and corrosion resistance of cast metal alloys.[18] Recently, however, it was suggested that magnesium aluminate (spinel, $MgAl_2O_4$) and magnesium oxide (MgO) can be potent substrates for enhanced heterogeneous nucleation of aluminum grains in aluminum–magnesium alloys, and as a result, uniform microstructure and fine grains can be achieved..[17,19,20] Accordingly, it is imperative to investigate their formation mechanism and ability to nucleate aluminum grains in order to facilitate the use of oxides for the grain refinement and structural uniformity of the alloys. $MgAl_2O_4$ with the density of 3.65 g/cm^3 exhibits a congruent melting point at 2315 °C in the MgO-Al_2O_3 phase diagram and shows low coefficient of thermal expansion, good thermal shock resistance, and high electrical resistivity.[21–23] The lattice parameter for the close-packed oxygen anion sublattice of the $MgAl_2O_4$ unit cell is nearly equal to that of aluminum unit cell with the same face-centered cubic structure. This similar crystal structure can form low energy interfaces for any orientation. For instance, the lattice mismatch of the $MgAl_2O_4$ (400) and aluminum (200) is about 0.2%, which is one of the lowest among all reinforcements in aluminum matrix.[21,24,25] Therefore, several studies suggested that a stable oxide that can act as the substrate for heterogeneous nucleation of aluminum grains is probably $MgAl_2O_4$.[17,20] However, it was shown that MgO (not $MgAl_2O_4$) can act as the substrate for

* *Correspondence to: K. H. Kim, School of Metallurgy and Materials, University of Birmingham, Edgbaston, Birmingham, West Midlands B15 2TT, UK.*
E-mail: kpsky3@gmail.com; k.kim.2@bham.ac.uk

School of Metallurgy and Materials, University of Birmingham, Edgbaston, Birmingham, West Midlands, B15 2TT, UK

the heterogeneous nucleation.[19] Because magnesium is a very effective surfactant to liquid aluminum, it has a high concentration at the surface of liquid aluminum–magnesium alloys.[17] The segregation of magnesium to the surface of liquid aluminum was detected experimentally in previous studies on the oxidation of molten aluminum.[17,26] Consequently, it is expected that the initial oxidation product of the aluminum–magnesium melt is MgO. In addition, it was shown by high-resolution analytical electron microscopy that MgO was detected at the center of one aluminum grain and might have acted as the substrate.[19] Therefore, it is necessary to investigate the formation mechanism of MgO and $MgAl_2O_4$ under normal melting conditions and their possibility of acting as substrates as the heterogeneous nucleation, which is the main purpose of this study. Furthermore, although many papers showed the interface of exogenous fiber or spinel/aluminum in aluminum-based composites,[3,6,8,9,11,13,27] there are few paper showing high-resolution analysis of the interface of endogenous oxide and aluminum. In this study, the interface has been also investigated by high-resolution analytical electron microscopy.

Experimental

Oxidation of aluminum alloys is dependent on oxidation time and temperature, alloying elements, and water vapor in oxidizing atmosphere.[16,28–31] Therefore, in this study, an aluminum alloy containing 4 wt.% magnesium, which previously showed the possibility of the enhanced heterogeneous nucleation of aluminum grains,[19,32] was used to minimize the effect of other alloying elements. Furthermore, the alloy was melted and held in dry air at a fixed temperature of 1023 K for 5 min (300 s), 17 min (1020 s), 1 h (3600 s), and 3 h (10 800 s). Samples were etched for 5 min in 2% HF solution and then melted in sintered alumina crucibles that were placed in an oxidation cell with dimensions 355 mm height and 48.4 mm diameter. The oxidation apparatus and procedure are outlined elsewhere.[33]

Surfaces of as-oxidized samples were observed by scanning electron microscopy (SEM). For cross-sectional observation, samples were submitted to standard cutting, grinding, and polishing operations. Microstructural observations were carried out with a field emission gun SEM (JEOL JSM-7000 F) equipped with an electron dispersive X-ray (EDX) spectrometer and a focused ion beam (FIB) SEM (FIB-SEM, FEI Quanta 3D) equipped with dual (ion and electron) beam and an EDX system. For high-resolution analytical electron microscopy, then, thin samples were fabricated by a FIB milling and lifting-out technique.[34–36] Figure 1 shows two representative sampling images by FIB. A sample showing a thin oxidized layer near the surface was selected for the sampling, and then, a protective tungsten layer was deposited on the marked region in Fig. 1a. The FIB lifting-out technique made trenches, thinned, and lifted out near the tungsten-deposited region. The region was then put on a copper grid and milled further for the transmission of electron beams in transmission electron microscopy (TEM). Figure 1b shows another sampling including fine particles. As indicated by the arrows, it is clear that the interested particles were fabricated into a TEM sample. Thin samples for TEM were observed by a high-resolution microscope (FE-TEM, FEI Tecnai F20) with a scanning mode [scanning transmission electron microscopy (STEM)] and an EDX system (STEM-EDX resolution 2~3 nm). Especially, for chemical analysis, STEM high angle annular dark field (HAADF) images using *Z*-contrast, which is directly related to the atomic number in the acquired region, were acquired in interested regions. For phase analysis, Trumap™ qualitative analysis software belonging to the EDX system, which can resolve a differences of more than 0.03 keV by the deconvolution of overlapping elements and background removal,[37] was used to measure the concentration and selected area diffraction patterns (SADP) were also used. For sufficient statistical

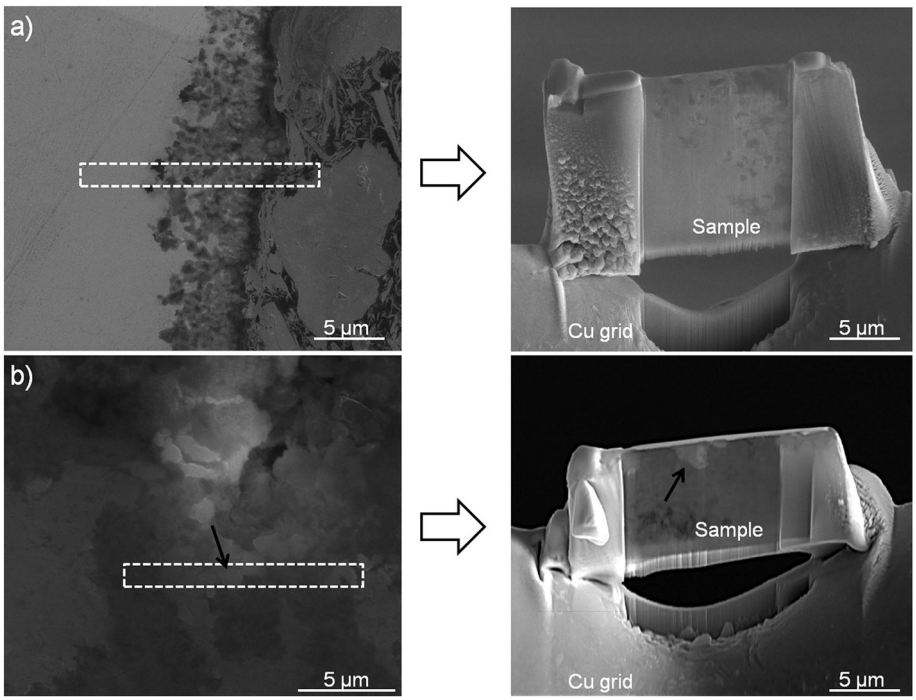

Figure 1. Two representative TEM samplings by a focused ion beam lift-out technique on an (a) oxidized layer and on (b) particles. Protective tungsten was deposited on the marked region in each panel. The arrows in (b) indicate the same particle.

confidence, all measurements were carried out on more than ten analysis areas. During TEM observation, every sample was cooled with liquid nitrogen to protect it from high energy electrons.

Results

High temperature oxidation of Al-4 wt.% Mg

Figure 2 shows typical SEM images of the cross-sections and surfaces Al-4 wt.% Mg alloy oxidized at 1023 K. A thin oxidized layer of about 5 μm forms initially on the surface of the alloy melt (Fig. 2a). As the oxidation time increases, the thickness of the layer increases gradually (Fig. 2c and e). At an extended oxidation time of about 3 h, the alloy is severely oxidized, and the oxidized thickness is over about 500 μm (Fig. 2g). Regardless of the oxidation time, the oxidized layer is not uniform. In order to know the morphology of as-oxidized sample for different oxidation times, the surfaces were observed at the same magnification of 1000×. The surface of an initially oxidized sample is quite porous (Fig. 2b). As the oxidation progresses, the porous morphology seems to disappear (Fig. 2d). However, the surface becomes serpentine (Fig. 2f), and finally, more deep and wide pores form (Fig. 2h).

For high-resolution analysis of the surfaces of as-oxidized samples, SEM images were also acquired at high magnifications of 50 000× (Fig. 3a and b) and 25 000× (Fig. 3c). At a short oxidation time of 5 min (Fig. 3a), granules of about several micrometers with numerous protrusions form and cover the surface. As oxidation progresses, a more complex morphology forms. However, SEM-EDX point analysis could not find any $MgAl_2O_4$ particles in shortly oxidized samples except MgO. As several studies suggested that $MgAl_2O_4$ phase forms after initial oxidation,[16,38] the surface oxidized for 3 h was scanned meticulously, and finally, a fine particle is detected as shown in Fig. 3b. The particle is clearly confirmed as $MgAl_2O_4$ after STEM-EDX analysis (see Fig. 6). In order to know the general morphology of $MgAl_2O_4$, the oxidation time was extended to 7 h. Figure 3c shows several $MgAl_2O_4$ particles. It is clear that $MgAl_2O_4$ exists as discrete particles near the surface. In addition, the size, which is an important parameter to evaluate the possibility of acting as the substrate for nucleation of aluminum grains, is diverse from about 100~200 nm to about 1~2 μm. Therefore, it is concluded that aluminum alloys melt containing magnesium oxidizes readily because of the high affinities of magnesium and aluminum with oxygen, forms initially MgO, and after initial oxidation, $MgAl_2O_4$ forms as discrete particles.

High-resolution observation of MgO

The particle detected in Fig. 3a was further investigated by TEM. The FIB technique described in Fig. 1 was used to make a TEM sample. Prior to the milling, a tungsten layer to protect the particle from strong gallium ion beam was deposited during TEM sampling. Figure 4 shows STEM-HAADF images and STEM-EDX element maps of the particle. The particle is preserved without any critical damage because of the protective tungsten deposition on its surface during the sampling (Fig. 4b). As expected, the particle is porous and composed of magnesium and oxygen (Fig. 4c and d). The magnified image (Fig. 4e) and element maps (Fig. 4f–h) of the interface of MgO/aluminum show that MgO and aluminum are contacted without any intermediate layer or any void between them. In order to confirm the intimate bonding between MgO and aluminum, another TEM sample was made from an oxidized specimen for 3 h. Figure 5 shows a STEM-HAADF image with SADP and STEM-EDX analysis of aluminum and MgO. As shown in Table 1, aluminum and MgO have nearly equal crystal structure and lattice parameters. Consequently, just with SADP, it is difficult to clearly distinguish aluminum with MgO even though several different diffraction patterns can be acquired at different zone axes. However, STEM-EDX analysis with resolution 2~3 nm clearly confirms and distinguishes the two phases (Fig. 5b and c). In Fig. 5, it is also confirmed that MgO and aluminum can be bonded directly even after the extensive oxidation. The intimate bonding is essential for MgO to act as the substrate for aluminum grains, which is discussed later.

High-resolution observation of $MgAl_2O_4$

Figures 2 and 3 showed that $MgAl_2O_4$ could form after initial oxidation time. In order to compare with the interface MgO/aluminum, that of $MgAl_2O_4$/aluminum was observed by high-resolution TEM. The $MgAl_2O_4$ particle detected in Fig. 3b was fabricated into a TEM sample by the FIB technique. Figure 6 is STEM-HAADF images and STEM-EDX element maps near the particle. The particle seems to be surrounded with MgO (Fig. 6a). However, STEM-HAADF images (Fig. 6b and f) and magnesium maps (Fig. 6c and g) acquired near the top surface and the bottom, respectively, of $MgAl_2O_4$ indicate that it seems there is an intermediate layer between MgO and $MgAl_2O_4$. In addition, aluminum and oxygen seem to exist in the intermediate layer. Figure 7 is STEM-EDX spectra of the marked points in Fig. 6b. The atomic percentages of each point are summarized in Table 2. The phases in the *point M* and the *point S* are MgO and $MgAl_2O_4$, respectively. The spectrum acquired at the *point A* corresponds clearly to aluminum oxide (Al_2O_3). Another TEM sample (Fig. 1b) made from a different specimen that had been oxidized for 7 h also showed the Al_2O_3 phase at the interface (not shown here). It is interesting to find Al_2O_3 at the interface of aluminum and $MgAl_2O_4$.

Figure 8 shows another interesting finding of Al_2O_3 near $MgAl_2O_4$. In this case, a $MgAl_2O_4$ particle that was detected near aluminum (not surrounded with MgO) was chosen for TEM sampling. A STEM-HAADF image shows clearly that there is another phase between *A* and *S* (Fig. 8a). Magnesium is detected in just the top region including the phase *S* (Fig. 8b). In contrast, aluminum shows different contrast through the whole region (Fig. 8c). It should be emphasized that the oxygen map does not correspond to the magnesium (Fig. 8d). STEM-EDX spectra show that the phases at the locations of *A* and *S* are aluminum and MgO, respectively. In addition, the phase at the location of *O* that is located between the two phases is aluminum oxide (Al_2O_3). Therefore, it is concluded that $MgAl_2O_4$ particles are covered with Al_2O_3, which means that even though $MgAl_2O_4$ seems to be contacted to aluminum, there is always an intermediate layer between $MgAl_2O_4$/aluminum or $MgAl_2O_4$/MgO, whereas MgO is bonded directly to aluminum.

Discussion

Formation of MgO and $MgAl_2O_4$ during high temperature oxidation

The formation energy of aluminum oxide (Al_2O_3) is extremely low as the following[39,40]:

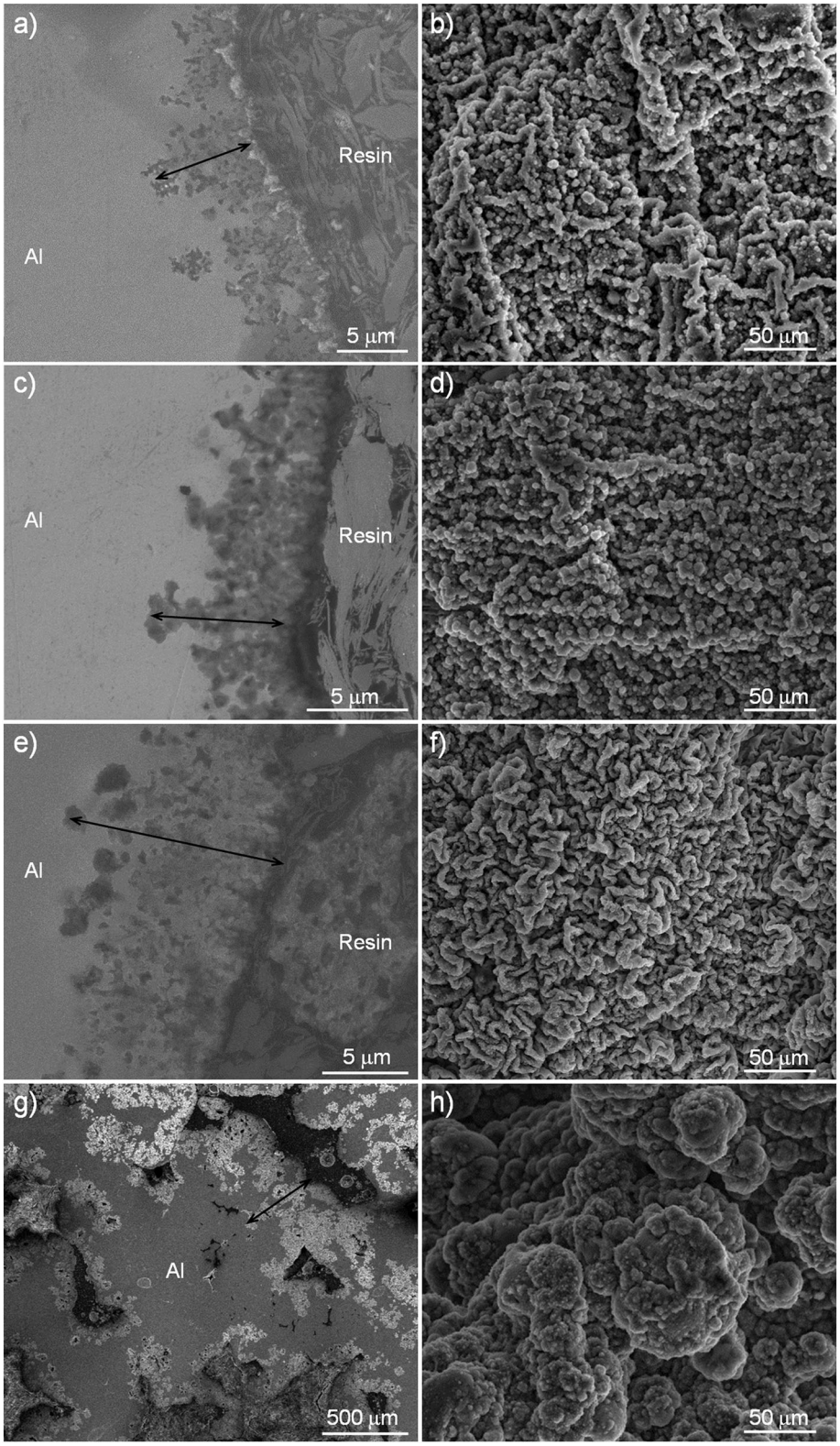

Figure 2. SEM images of cross-sections (a, c, e, and g) and top views (b, d, f, and h) of oxidized samples for (a and b) 5 min, (c and d) 17 min, (e and f) 1 h, and (g and h) 3 h.

$$2Al_{(l)} + \frac{3}{2}O_{2(g)} = Al_2O_{3(s)}$$

$$\Delta G^0_{1023K} = -1348.64 kJ/mol$$

However, magnesium oxide (MgO) forms more easily than Al_2O_3 because of the higher reactivity of magnesium than aluminum and the preferential segregation of magnesium atoms at the interface or surface.[21] Therefore, the initial oxidation product of aluminum

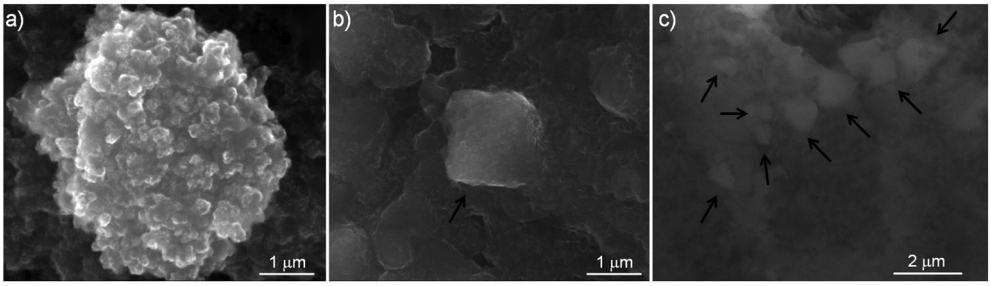

Figure 3. Magnified high-resolution SEM images of as-oxidized surfaces for (a) 5 min, (b) 3 h, and (c) 7 h. Note that the arrows, respectively, in (b) and (c) indicate $MgAl_2O_4$.

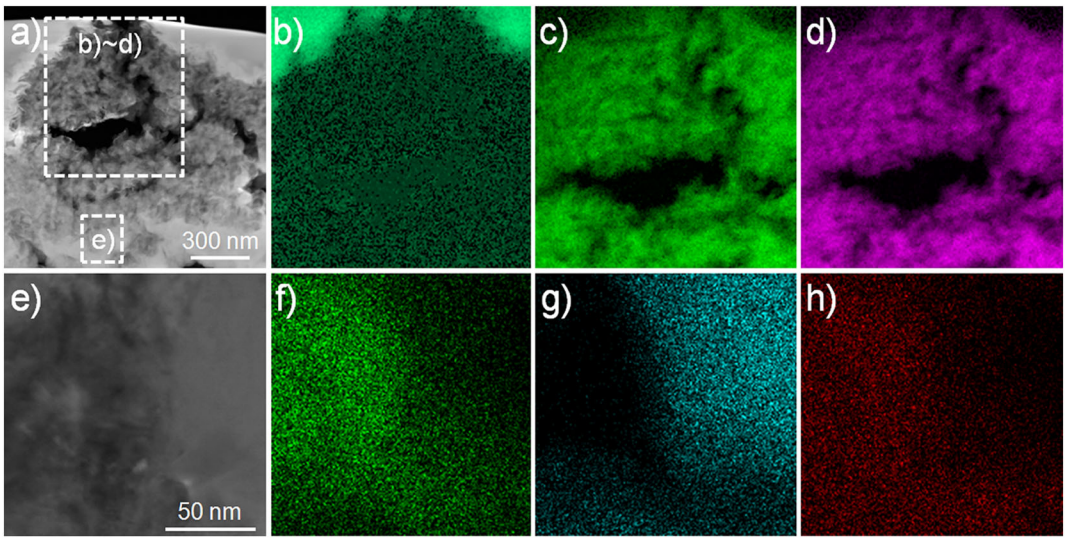

Figure 4. TEM analysis of MgO formed for 5 min: (a) STEM-HAADF image near the oxidized layer, (b–d) STEM-EDX element maps of (b) tungsten, (c) magnesium, and (d) oxygen, and (e–h) STEM-HAADF image (e) and corresponding STEM-EDX maps of (f) magnesium, (g) aluminum, and (h) oxygen at the marked region in (a).

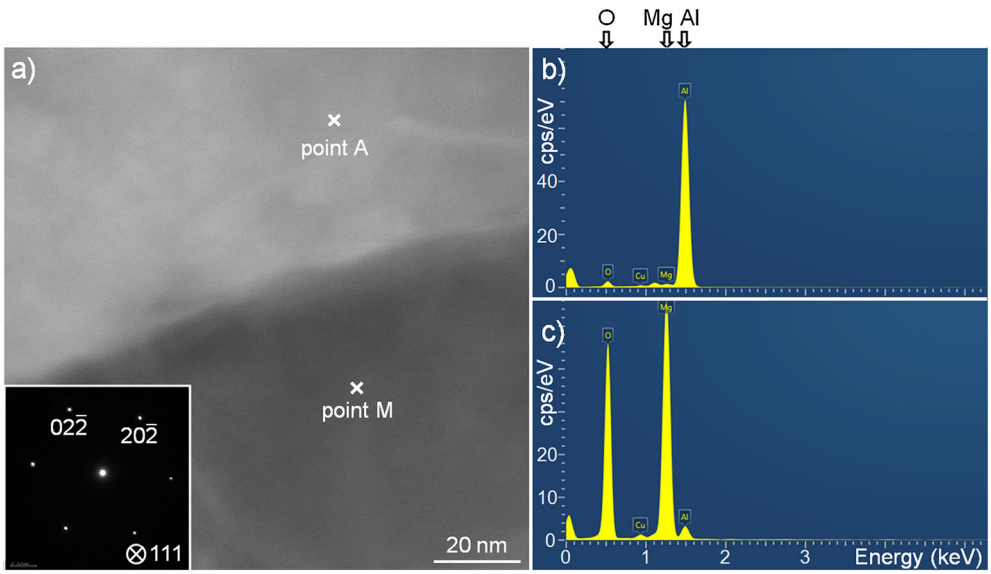

Figure 5. TEM analysis of MgO formed for 3 h: (a) STEM-HAADF image with SADP corresponding to MgO, and (b and c) STEM-EDX spectra of at the (b) *point A* and the (c) *point M* in panel (a). Note that the peaks of copper were generated from the TEM grid.

Table 1. Crystal structures of aluminum and some aluminum and/or magnesium oxides, and lattice disregistry with aluminum[31,46,63]

Phase	Space group	Crystal system	Lattice parameters and angle (nm)	Lattice disregistry with Al (%)	Lattice disregistry with specific OR
Al	$Fm\bar{3}m$	Cubic	a = 0.4050	0	0
α-Al_2O_3	$R\bar{3}c$	Hexagonal	a = 0.4758; c = 1.2991; $\gamma = 120°$	4.2	4.2[a]
γ-Al_2O_3	$Fd\bar{3}m$	Cubic	a = 0.7859	3	3.4[b]
$MgAl_2O_4$	$Fd\bar{3}m$	Cubic	a = 0.8075	3.1	1.4[b]
MgO	$Fm\bar{3}m$	Cubic	a = 0.4213	3.9	3.1[b]

[a]The orientation relationship is $(111)_{Al}[\bar{1}10]_{Al}//(0001)_{Al_2O_3}[10\bar{1}0]_{Al_2O_3}$.
[b]The orientation relationship is $\{111\}_{Al} < 110 >_{Al}//\{111\}_{Oxide} < 110 >_{Oxide}$.

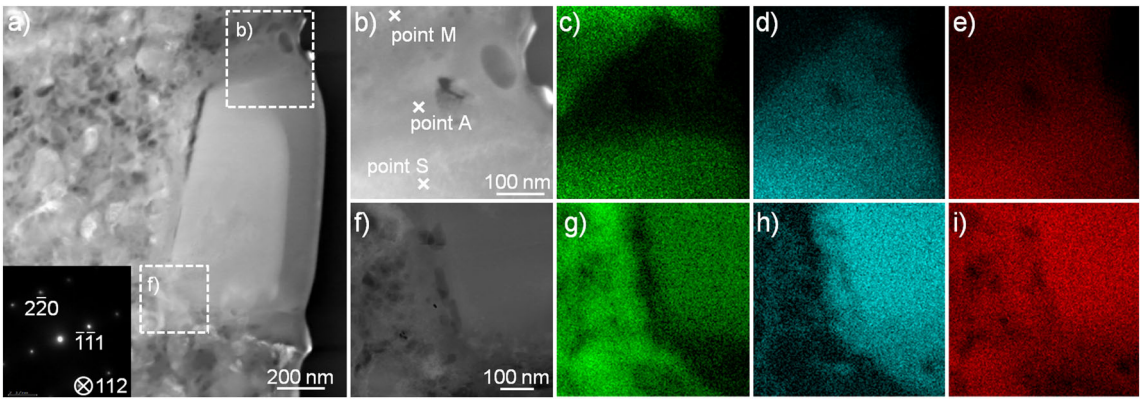

Figure 6. TEM analysis of a $MgAl_2O_4$ particle formed for 3 h: (a) STEM-HAADF image near the particle with a SADP acquired on $MgAl_2O_4$, and (b–i) STEM-HAADF image (b and f) and corresponding STEM-EDX element maps of (c and g) magnesium, (d and h) aluminum, and (c and i) oxygen at the marked regions in panel (a).

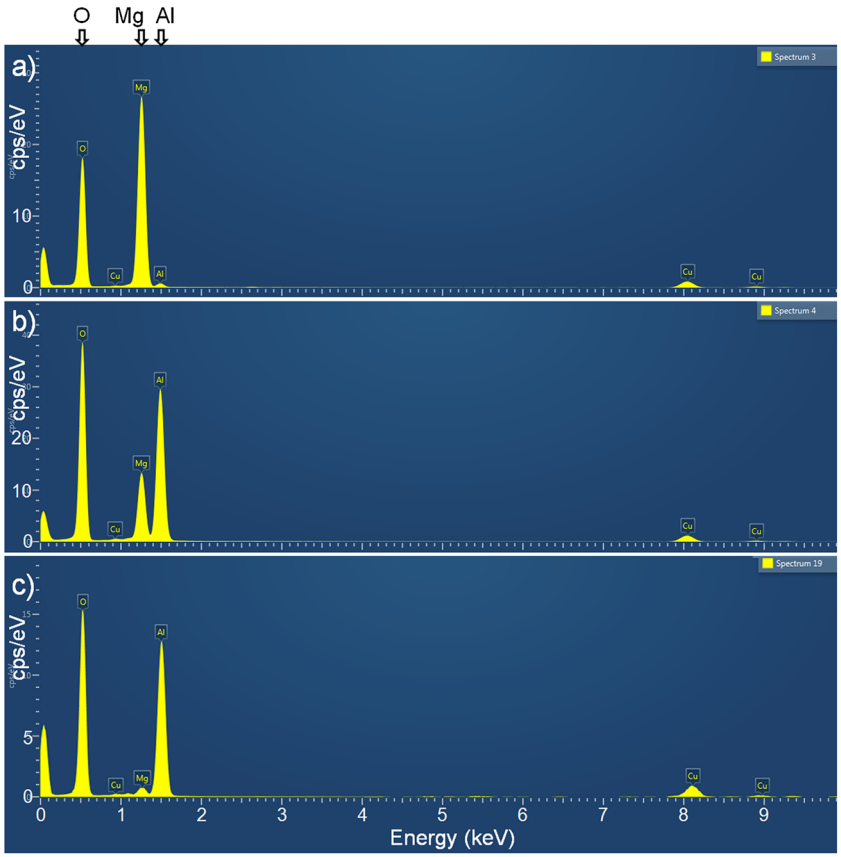

Figure 7. STEM-EDX spectra at the (a) *point M*, (b) *point S*, and (c) *point A* in Fig. 6b.

Table 2. STEM-EDX point analysis at *point M*, *S*, and *A* in Fig. 6a

Point	Element content (%)			Phase
	Mg	Al	O	
M	43	≤1	56	MgO
S	11	23	64	$MgAl_2O_4$
A	≤1	36	63	Al_2O_3

melt containing magnesium is MgO at 1023 K by the following reaction[17,39]:

$$3Mg_{(l)} + \frac{3}{2}O_{2(g)} = 3MgO_{(s)}$$
$$\Delta G^0_{1023K} = -1471.17kJ/mol$$

The formation of MgO means that magnesium near the surface of aluminum–magnesium melt is selectively oxidized and, consequently, it produces porous MgO.[16] Through porous structure, oxygen in air can be introduced into the melt, and consequently, more MgO forms and disperses irregularly near the surface of the melt (Fig. 2). After that, as shown previously, $MgAl_2O_4$ forms after the initial formation of MgO. Compared with the formations of Al_2O_3 and MgO, the mechanism of $MgAl_2O_4$ formation is more complex, and consequently, many different reactions have been introduced. The following reaction, based on thermodynamic considerations, is suggested for the formation of the spinel phase on the surface of the liquid metal because of voracious oxygen affinity[6]:

$$\frac{3}{4}Mg_{(l)} + \frac{3}{2}Al_{(l)} + \frac{3}{2}O_{2(g)} = \frac{3}{4}MgAl_2O_{4(s)}$$
$$\Delta G^0_{1023K} = -1222.19kJ/mol$$

In this study, $MgAl_2O_4$ formed during the extended oxidation shows the morphology of discrete particles instead of continuous film. It is well known that if the Pilling–Bedworth ratio under an assumption of oxygen diffusion through the oxide layer, which is expressed as V_{ox}/V_m where V_{ox} and V_m that are the oxide volume produced and metal volume consumed, respectively, is less than 1, the oxide layer exists as discrete particles (not a continuous layer).[17,41–43] Because the value of MgO is 0.73 for aluminum, the oxide layer tends to be porous and shows the morphology of discrete particles. By contrast, if $MgAl_2O_4$ is formed by the reaction of aluminum and magnesium with oxygen, the value is 1.30, which means the oxide should form a continuous film. However, the current experimental observation showed that $MgAl_2O_4$ exists as discrete particles near the surface of melt. Similarly, $MgAl_2O_4$ formed in an Al-0.7 Mg alloy also showed the morphology of discrete particles.[17] Therefore, $MgAl_2O_4$ formed after initial oxidation in this study might form by different reaction(s) not by the direct reaction of $Al + Mg + O$. There are other possible reactions for the formation of $MgAl_2O_4$ at the interface of MgO/aluminum or Mg/Al_2O_3 if Al_2O_3 exists[3,4,9,21]:

$$3Mg_{(l)} + 4Al_2O_{3(s)} = 3MgAl_2O_{4(s)} + 2Al_{(l)}$$
$$\Delta G^0_{1023K} = -236.01kJ/mol$$
$$MgO_{(s)} + 2Al_{(l)} + \frac{3}{2}O_{2(g)} = MgAl_2O_{4(s)}$$
$$\Delta G^0_{1023K} = -1139.19kJ/mol.$$

In addition, because Al_2O_3 reacts readily with divalent transition metal oxides to form spinel aluminates,[9,44] the following reaction is also possible[3,11]:

$$MgO_{(s)} + Al_2O_{3(s)} = MgAl_2O_{4(s)}$$
$$\Delta G^0_{1023K} = -37.32kJ/mol.$$

As this reaction involves a solid-state reaction, if occurred in this study, this process might be kinetically slow.[9]

It was suggested that dispersed Al_2O_3 particles can act as the sites of the formation of $MgAl_2O_4$.[44] However, even in this case, a boundary layer between the Al_2O_3 particles and the matrix was observed by electron microscopy, which means that the direct reaction of MgO and Al_2O_3 is probably difficult. In addition, as shown in Fig. 6, $MgAl_2O_4$ was not detected between MgO and Al_2O_3. Therefore, the $MgAl_2O_4$ phase in this study might be formed by the reactions of $Mg + Al_2O_3$ or $MgO + Al + O$. The reaction of magnesium or aluminum with MgO or Al_2O_3 was also suggested in fiber-reinforced metal matrix composites.[9,13] Comparing the formation of MgO from magnesium and oxygen, the absolute value of Gibbs' free energy for the reaction of $Mg + Al_2O_3$ is small. In addition, MgO is porous, which means that the inside magnesium or MgO can meet oxygen that is introduced from air through the porous structure. Therefore, the reaction of $Mg + Al_2O_3$ is not energetically favorable because of the strong reaction of $Mg + O$. The remaining reaction for the formation of $MgAl_2O_4$ is MgO + Al + O. Even though the reaction of MgO with aluminum requires the presence of oxygen, the reaction is favorable because of the porous morphology of MgO. From the initial oxidation, numerous MgO has already formed, and most of all, the solid MgO is surrounded with liquid aluminum. Therefore, if oxygen in air can be introduced through the porous MgO and met with MgO and aluminum at their interface, $MgAl_2O_4$ can form easily from the reaction of MgO + Al + O. However, this reaction is competitive with the oxidation reaction of aluminum with oxygen. Consequently, when oxygen meets MgO and aluminum at their interface, two reactions may occur together as shown in Fig. 9: the reaction of MgO + Al + O on the side of MgO and the aluminum oxidation on the side of aluminum melt. As a result, $MgAl_2O_4$ can be covered with Al_2O_3, as shown in Figs. 6 and 8. It should be noted that as the Pilling–Bedworth ratio of Al_2O_3 is 1.29,[41] the oxide layer exists as a continuous layer on aluminum. If the coverage of Al_2O_3 did not happen in this study, the following reactions might occur:

$$2Al_{(l)} + 2MgAl_2O_{3(s)} \rightarrow 3Al_2O_{3(s)} + 2MgO_{(s)}$$
$$\Delta G^0_{1023K} = -203.58kJ/mol$$
$$3Mg_{(l)} + MgAl_2O_{4(s)} \rightarrow 4MgO_{(s)} + 2Al_{(l)}$$
$$\Delta G^0_{1023K} = -86.81kJ/mol$$

As a result, instead of the pure Al_2O_3 in Figs. 6 and 8, MgO or the mixture of MgO and Al_2O_3 should have been detected near the $MgAl_2O_4$.

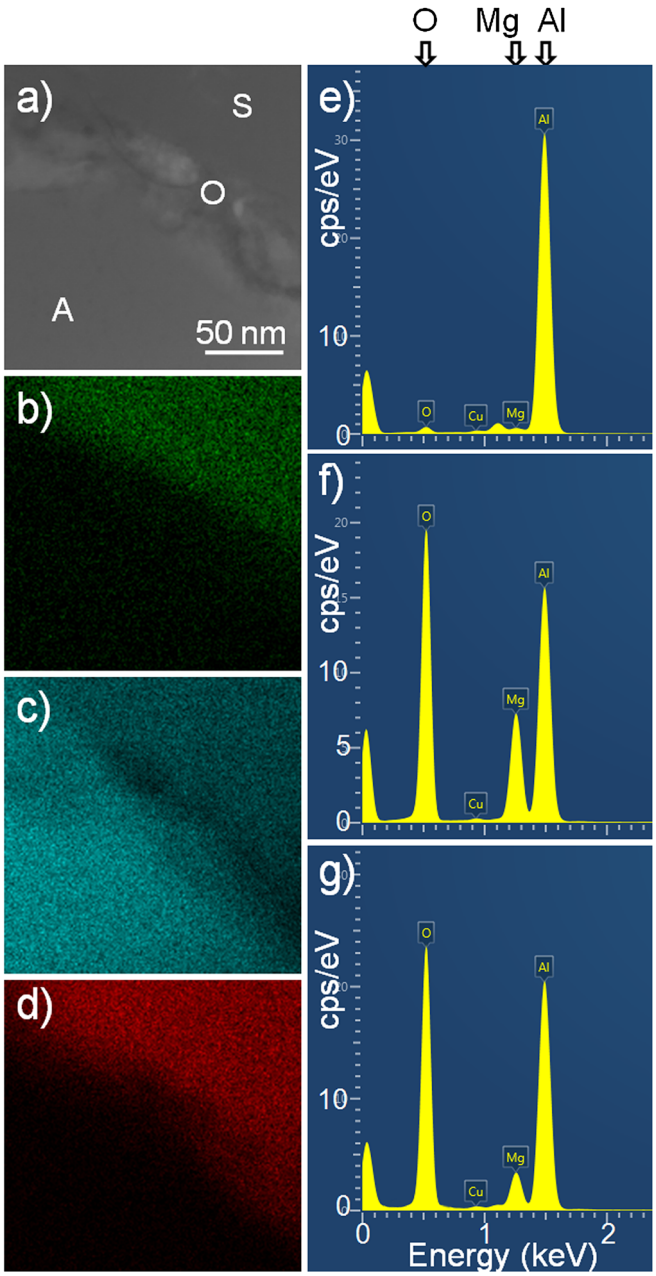

Figure 8. TEM analysis of $MgAl_2O_4$ formed for 3 h: (a–d) STEM-HAADF image (a) and corresponding STEM-EDX element maps of (b) magnesium, (c) aluminum, and (d) oxygen near the interface of MgO and aluminum, (e–g) STEM-EDX spectra of at the points (e) *A*, (f) *S*, and (g) *O*, respectively, in panel (a).

Possibility of MgO and $MgAl_2O_4$ as substrates for heterogeneous nucleation of aluminum grains

The coverage of Al_2O_3 on the surface of $MgAl_2O_4$ can affect significantly the ability of $MgAl_2O_4$ to nucleate heterogeneously aluminum grains. In classical heterogeneous nucleation theory based on a spherical cap model, the activation energy barrier against heterogeneous nucleation is mainly dependent on the interfacial energy of nucleant/nucleus metal and the shape of the nucleus.[45] Accordingly, good crystallographic match between the nucleant and the nucleus metal is significantly considered for a low interfacial energy, which can be achieved by small disregistry and similar crystallography.[46] The lattice disregistry (δ) between particles and metallic grains with the same crystal structure is simply defined as follows:[47,48]

$$\delta = \frac{|a_p - a_m|}{\left(\frac{a_p + a_m}{2}\right)}$$

where a_p and a_m are the lattice parameters of the particle and the nucleating metallic phase, respectively. Because α-Al_2O_3 has the different crystal structure with aluminum but has the orientation relationship with aluminum, such as $(111)_{Al}\left[\bar{1}10\right]_{Al}//(0001)_{Al_2O_3}\left[10\bar{1}0\right]_{Al_2O_3}$ and $(111)_{Al}\left[\bar{1}2\bar{1}\right]_{Al}//(0001)_{Al_2O_3}\left[2\bar{1}\bar{1}0\right]_{Al_2O_3}$, the lattice disregistry between aluminum and α-Al_2O_3 can be expressed as follows[49]:

$$\delta = 2\cdot\frac{\sqrt{\frac{3}{2}}\cdot a_m - a_{Al_2O_3}}{\sqrt{\frac{3}{2}}\cdot a_m + a_{Al_2O_3}}$$

where $a_{Al_2O_3}$ is the lattice parameter of α-Al_2O_3. Table 1 is estimated values for aluminum and/or magnesium oxides. Because the oxide phases with cubic crystal structure have the orientation relationship with aluminum, such as $\{111\}_{Al}<110>_{Al}//\{111\}_{Oxide}<110>_{Oxide}$, the lattice disregistry along with these planes and directions was also estimated. Even though α-Al_2O_3 and γ-Al_2O_3 have low values of the lattice disregistry with aluminum, as already discussed, MgO forms more easily than Al_2O_3 because of the high reactivity of magnesium and preferential segregation of magnesium atoms. Therefore, MgO and $MgAl_2O_4$ have high potencies of the nucleation because of their low lattice mismatch and the same face-centered cubic structures with aluminum.[19,50]

Recently, however, experimental observations using high-resolution TEM suggested that nucleation of metal on an oxide commences at atomic level.[51–53] Furthermore, Fan introduced a new model for heterogeneous nucleation on potent substrates.[54] Beyond a critical undercooling, epitaxial growth of a pseudomorphic layer takes place at atomic level on a potent substrate. Kim also introduced that atomic level bonding across the interface of nucleant/nucleus is important for the heterogeneous nucleation.[19] As $MgAl_2O_4$ has a cube-on-cube orientation relationship with aluminum,[17] the particle is considered as a high potential oxide for the nucleation of aluminum grains. However, Figs. 6 and 8 showed that $MgAl_2O_4$ particles are clearly covered with Al_2O_3. Thus, as nucleation of aluminum grains commences at atomic level, if occurred, the nucleation of aluminum grains could occur on the surface of Al_2O_3 not on $MgAl_2O_4$. Without the coverage of Al_2O_3, $MgAl_2O_4$ might act easily as the substrate.

MgO forms initially near the surface of the aluminum–magnesium melt. When MgO forms, it contacts directly to the melt. As shown in Fig. 2, numerous MgO were detected near the surface of melt, and furthermore, they were bonded intimately to aluminum as shown in Figs. 4 and 5, despite the thermal stress between the ceramic MgO and the metallic matrix that was caused by their different thermal conductivities.[55–57] In addition, it was suggested that strong bonds between oxygen-terminated MgO and aluminum are generated by the ionic component and covalent/metallic contribution because of the change of the electron density of oxygen atoms at the top layer of MgO.[52] Therefore, MgO particles have high possibility of acting as the substrate of nucleation of aluminum grains. Recently, Kim experimentally showed the ability of MgO to nucleate aluminum grains in an intensively sheared aluminum alloy.[19] Furthermore, the observation of dendritic growth of aluminum from the surface of aluminum–magnesium

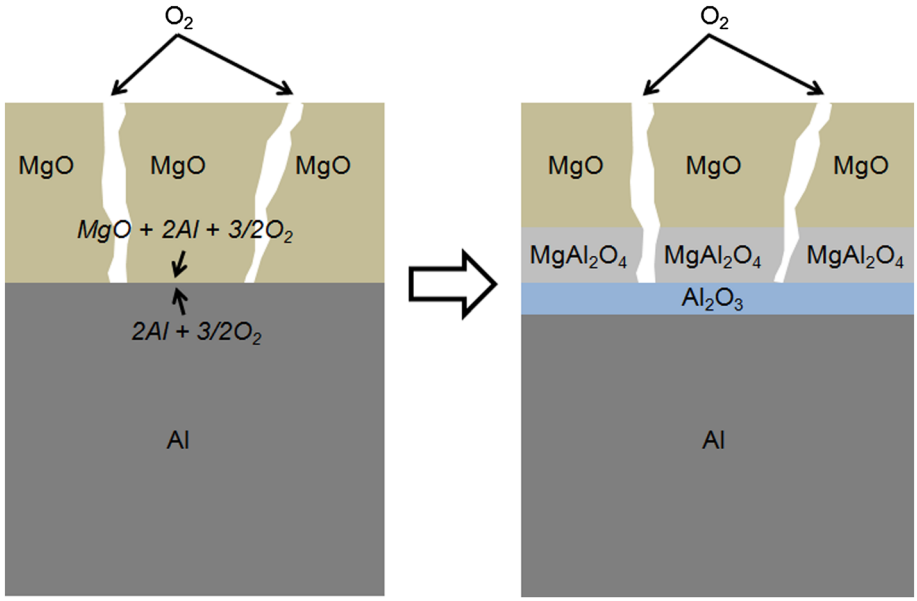

Figure 9. Schematic diagram of the formation reactions of $MgAl_2O_4$ and Al_2O_3 at the interface of MgO and aluminum melt. Note that the spurting and oxidation of aluminum melt through the porous structure of MgO is not expressed in the figure for simplicity.

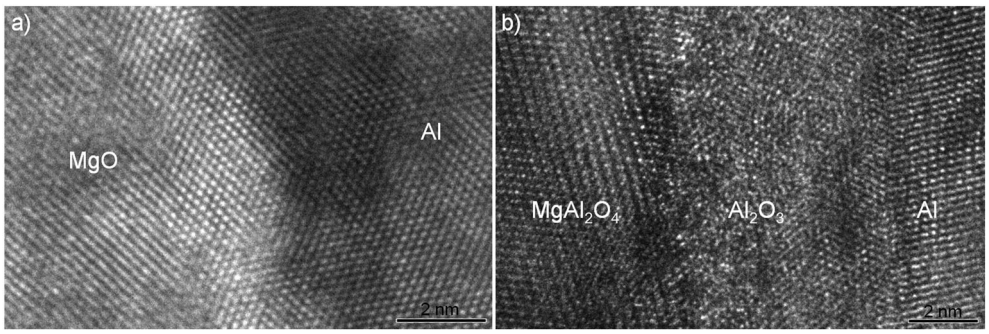

Figure 10. High-resolution lattice images by TEM at the interface of (a) Al/MgO and (b) $MgAl_2O_4/Al_2O_3$/MgO.

melt also suggested the possibility of MgO as a nucleant for nucleation of aluminum.[33]

Finally, high-resolution lattice images by TEM at the interface of Al/MgO and $MgAl_2O_4$/ Al_2O_3/MgO (Fig. 10) clarifies the ability of MgO and $MgAl_2O_4$ to nucleate aluminum grains at atomic level. MgO and aluminum are intimately bonded without any gap or intermediate layer, whereas Al_2O_3 prevents the direct contact of $MgAl_2O_4$ and aluminum. Therefore, it is concluded that when MgO particles surrounded with liquid aluminum are cooled down, they can act directly as the substrate of nucleation of aluminum grains. In contrast, for $MgAl_2O_4$, the intermediate layer of Al_2O_3 must be removed, or the particle of $MgAl_2O_4$ should be broken to reveal its fresh surface to act directly as the substrate. However, as the size of particles decreases, more undercooling is necessary to nucleate aluminum grains. Greer *et al.* introduced the following relation of the undercooling (ΔT_g) necessary for the free growth of aluminum and the diameter (d) of nucleant particles[58,59]:

$$\Delta T_g = \frac{4\gamma_{sl}}{\Delta S_f \cdot d}$$

where γ_{sl} is the interface energy of solid/liquid and ΔS_f is the fusion entropy per unit volume. Furthermore, they suggested that the optimum size of particles is about 2 μm,[59] which is almost the same size of $MgAl_2O_4$ particles formed naturally during oxidation in this study. Therefore, if $MgAl_2O_4$ particles are broken by any additional mechanical process, such as melt conditioning using intensive shearing[18,32,60] or electromagnetic stirring,[61,62] the size deviates from the optimum. First of all, more undercooling is necessary for the free growth of aluminum, which means that the ability of $MgAl_2O_4$ to nucleate aluminum grains decreases.

Summaries and conclusion

Aluminum containing 4 wt.% magnesium was oxidized at 750 °C for different lengths of time. MgO formed initially near the surface of aluminum–magnesium melt, and they were covered with aluminum. After extended oxidation time, discrete $MgAl_2O_4$ particles formed. Even though the mechanism of $MgAl_2O_4$ formation was complex, the observation in this study suggested that the particles were formed by the reaction of initially formed MgO, liquid aluminum, and oxygen that was introduced from air through the porous MgO. High-resolution analytical electron microscopy revealed that $MgAl_2O_4$ particles were covered with Al_2O_3, which means that $MgAl_2O_4$ particles that form naturally during oxidation are difficult

to act as a direct substrate for nucleation of aluminum grains. In contrast, MgO was bonded intimately to aluminum and showed the possibility of acting as a substrate for the aluminum nucleation.

This study suggested that nucleation of aluminum grains on large amounts of MgO is more effective than that on $MgAl_2O_4$ covered with Al_2O_3 that forms after incubation time. In addition, it was confirmed that it is necessary to consider atomic level bonding and mismatches of nucleant/nucleus metal for correct evaluation of the possibility of heterogeneous nucleation of metallic matrix on a potent nucleant. These atomic level observations and models may explain the well-known low efficiency of inoculants in aluminum or magnesium casting. Because the nucleation begins at atomic level, the chemical state of atoms and impurities at the surface of inoculants can affect significantly the nucleation and consequently the efficiency of inoculants.

Acknowledgements

The author thanks Dr W. D. Griffiths and Ms E. Hinton of the University of Birmingham for supplying the material for investigation, the EPSRC Centre for Innovative Manufacturing in Liquid Metal Engineering (EP/H026177/1) for financial support, and particularly Mrs Susan Jackson, Mr Minjoon Kim, and Mrs Sunyoung Park for manuscript preparation.

References

[1] B. C. Pai, G. Ramani, R. M. Pillai, K. G. Satyanarayana, *J. Mater. Sci.* **1995**, *30*, 1903.
[2] J. Hashim, L. Looney, M. S. J. Hashmi, *J. Mater. Process. Tech.* **1999**, *92–93*, 1.
[3] J. C. Lee, K. N. Subramanian, Y. Kim, *J. Mater. Sci.* **1994**, *29*, 1983.
[4] P. Shen, D. Zhang, Q.-L. Lin, L.-X. Shi, Q.-C. Jiang, *Metall. Mater. Trans. A* **2010**, *41*, 1621.
[5] H. Watanabe, T. Saitoh, *J. Jpn Inst. Light Met.* **1989**, *39*, 262.
[6] A. Papworth, P. Fox, *Mater. Sci. Technol.* **1997**, *13*, 912.
[7] C. B. Carter, Y. K. Rasmussen, *Acta Metall. Mater.* **1994**, *42*, 2729.
[8] K. B. Lee, H. S. Sim, Y. S. Kim, J. H. Han, H. Kwon, *J. Mater. Sci.* **2002**, *37*, 1845.
[9] C. Levi, G. Abbaschian, R. Mehrabian, *Metall. Mater. Trans. A* **1978**, *9*, 697.
[10] C.-M. Liu, J.-C. Chen, C.-J. Chen, *J. Cryst. Growth* **2006**, *292*, 302.
[11] R. Mogilevsky, S. R. Bryan, W. S. Wolbach, T. W. Krucek, R. D. Maier, G. L. Shoemaker, J. M. Chabala, K. K. Soni, R. Levi-Setti, *Mater. Sci. Eng. A* **1995**, *191*, 209.
[12] A. Munitz, M. Metzger, R. Mehrabian, *Metall. Trans. Phys. Metall. Mater. Sci.* **1979**, *10*, 1491.
[13] K. Suganuma, T. Okamoto, T. Hayami, Y. Oku, N. Suzuki, *J. Mater. Sci.* **1988**, *23*, 1317.
[14] S. Chu, R. Wu, *Compos. Sci. Tech.* **1999**, *59*, 157.
[15] C. Cochran, D. Belitskus, D. Kinosz, *Metall. Mater. Trans. B* **1977**, *8*, 323.
[16] I. Haginoya, T. Fukusako, *Trans. J. Inst. Met.* **1983**, *24*, 613.
[17] H. T. Li, Y. Wang, Z. Fan, *Acta Mater.* **2012**, *60*, 1528.
[18] Y. Zuo, H. Li, M. Xia, B. Jiang, G. M. Scamans, Z. Fan, *Scr. Mater.* **2011**, *64*, 209.
[19] K. Kim, *Mater. Lett.* **2014**, *117*, 74.
[20] Y. Wang, H. T. Li, Z. Y. Fan, *Trans. Indian Inst. Met.* **2012**, *65*, 653.
[21] V. M. Sreekumar, R. M. Pillai, B. C. Pai, M. Chakraborty, *Appl. Phys. Mater. Sci. Process.* **2008**, *90*, 745.
[22] L. Rooi Ping, A.-M. Azad, T. Wan Dung, *Mater. Res. Bull.* **2001**, *36*, 1417.
[23] R. Caracas, E. J. Banigan, *Phys. Earth Planet. In.* **2009**, *174*, 113.
[24] S. B. Sinnott, E. C. Dickey, *Mater. Sci. Eng. R Rep.* **2003**, *43*, 1.
[25] R. Schweinfest, S. Köstlmeier, F. Ernst, C. Elsäser, T. Wagner, M. W. Finnis, *Phil. Mag. A* **2001**, *81*, 927.
[26] E. Bergsmark, C. J. Simensen, P. Kofstad, *Mater. Sci. Eng. A* **1989**, *120–121*, 91.
[27] H. J. Dudek, A. Kleine, R. Borath, G. Neite, *Mater. Sci. Eng. A* **1993**, *167*, 129.
[28] P. E. Blackburn, E. A. Gulbransen, *J. Electrochem. Soc.* **1960**, *107*, 944.
[29] A. Robertson, A. J. Rostron, *Corros. Sci.* **1965**, *5*, 425.
[30] Y. Wang, M. Xia, Z. Fan, X. Zhou, G. E. Thompson, *Intermetallics* **2010**, *18*, 1683.
[31] L. F. Mondolfo, *Aluminium Alloys: Structure and Properties*, Butterworth, London, **1976**.
[32] S. Kumar, N. Hari Babu, G. M. Scamans, Z. Fan, *Mater. Sci. Technol.* **2011**, *27*, 1833.
[33] E. M. Hinton, W. D. Griffiths, N. R. Green, *Mater. Sci. Forum* **2013**, *765*, 180.
[34] K. Kim, M. Watanabe, K. Mitsuishi, K. Iakoubovskii, S. Kuroda, *J. Phys. D Appl. Phys.* **2009**, *42*, 065304.
[35] K. Kim, S. Kuroda, M. Watanabe, *J. Therm. Spray Techn.* **2010**, *19*, 1244.
[36] K. Kim, M. Watanabe, S. Kuroda, N. Kawano, *Mater. Trans.* **2011**, *52*, 439.
[37] Oxford Instruments, AZtecEnergy: The Ultimate EDS System, **2013**.
[38] G. M. Scamans, E. P. Butler, *Metall. Trans. A* **1975**, *6*, 2055.
[39] Y. K. Rao, *Stoichiometry and Thermodynamics of Metallurgical Processes*, Cambridge University Press, Cambridge, **2009**.
[40] D. R. Gaskell, *Introduction to Metallurgical Thermodynamics*, McGraw-Hill, New York, **1981**.
[41] N. B. Pilling, R. E. Bedworth, *J. Inst. Met.* **1923**, *29*, 529.
[42] C. Xu, W. Gao, *Mater. Res. Innovat.* **2000**, *3*, 231.
[43] W. Ha, Y.-J. Kim, *J. Alloys Compd.* **2006**, *422*, 208.
[44] A. N. Abdel-Azim, Y. Shash, S. F. Mostafa, A. Younan, *J. Mater. Process. Tech.* **1995**, *55*, 199.
[45] D. A. Porter, K. E. Eastering, M. Y. Sherif, *Phase Transformations in Metals and Alloys*, Third ed., CRC Press, Boca Raton, **2009**.
[46] B. Bramfitt, *Metall. Trans.* **1970**, *1*, 1987.
[47] J. G. Conley, M. E. Fine, J. R. Weertman, *Acta Metall.* **1989**, *37*, 1251.
[48] B. Geddes, H. Leon, X. Huang, *Superalloys: Alloying and Performance*, ASM International, Materials Park, Ohio, **2010**.
[49] G. Pilania, B. J. Thijsse, R. G. Hoagland, I. Lazic, S. M. Valone, X.-Y. Liu, *Sci. Rep.* **2014**, 4.
[50] X. Cao, J. Campbell, *Metall. Mater. Trans. A* **2003**, *34*, 1409.
[51] N. Shibata, A. Goto, K. Matsunaga, T. Mizoguchi, S. D. Findlay, T. Yamamoto, Y. Ikuhara, *Phys. Rev. Lett.* **2009**, *102*, 136105.
[52] T. Hong, J. R. Smith, D. J. Srolovitz, *Acta Metall. Mater.* **1995**, *43*, 2721.
[53] S. H. Oh, Y. Kauffmann, C. Scheu, W. D. Kaplan, M. Rühle, *Science* **2005**, *310*, 661.
[54] Z. Y. Fan, *Metall. Mater. Trans. A* **2013**, *44A*, 1409.
[55] A. E. Karantzalis, A. Lekatou, E. Georgatis, T. Tsiligiannis, H. Mavros, *J. Mater. Eng. Perform.* **2010**, *19*, 1268.
[56] W. Zhou, Z. M. Xu, *J. Mater. Process. Tech.* **1997**, *63*, 358.
[57] S. Kuroda, T. W. Clyne, *Thin Solid Films* **1991**, *200*, 49.
[58] H. Men, B. Jiang, Z. Fan, *Acta Mater.* **2010**, *58*, 6526.
[59] A. L. Greer, A. M. Bunn, A. Tronche, P. V. Evans, D. J. Bristow, *Acta Mater.* **2000**, *48*, 2823.
[60] Z. Fan, B. Jiang, Y. Zuo, Apparatus and method for liquid metals treatment, US 20130228045 A1, **2013**.
[61] W. Braunbek, *Zeitschrift für Physik* **1932**, *73*, 312.
[62] V. Metan, K. Eigenfeld, *Eur. Phys. J. Spec. Top.* **2013**, *220*, 139.
[63] J. F. Grandfield, D. G. Eskin, I. Bainbridge, *Direct-chill Casting of Light Alloys: Science and Technology*, Wiley, Hoboken, New Jersey, **2013**.